

# ObjectAug: Object-level Data Augmentation for Semantic Image Segmentation

Jiawei Zhang, Yanchun Zhang, and Xiaowei Xu

Shanghai key Laboratory of Data Science, School of Computer Science, Fudan University, Shanghai, China

College of Engineering and Science, Victoria University, Melbourne, Australia

Guangdong Cardiovascular Institute, Guangdong Provincial People's Hospital, Guangzhou, China

17110240008@fudan.edu.cn, yanchun.zhang@vu.edu.au, xiao.wei.xu@foxmail.com

## Abstract

Semantic image segmentation aims to obtain object labels with precise boundaries, which usually suffers from overfitting. Recently, various data augmentation strategies like regional dropout and mix strategies have been proposed to address the problem. These strategies have proved to be effective for guiding the model to attend on less discriminative parts. However, current strategies operate at the image level, and objects and the background are coupled. Thus, the boundaries are not well augmented due to the fixed semantic scenario. In this paper, we propose ObjectAug to perform object-level augmentation for semantic image segmentation. ObjectAug first decouples the image into individual objects and the background using the semantic labels. Next, each object is augmented individually with commonly used augmentation methods (e.g., scaling, shifting, and rotation). Then, the black area brought by object augmentation is further restored using image inpainting. Finally, the augmented objects and background are assembled as an augmented image. In this way, the boundaries can be fully explored in the various semantic scenarios. In addition, ObjectAug can support category-aware augmentation that gives various possibilities to objects in each category, and can be easily combined with existing image-level augmentation methods to further boost performance. Comprehensive experiments are conducted on both natural image and medical image datasets. Experiment results demonstrate that our ObjectAug can evidently improve segmentation performance.

## Introduction

Semantic segmentation with the goal to assign semantic labels to target objects in an image is one of the fundamental topics in computer vision. Recently, Deep neural networks (DNNs) have been widely adopted in semantic segmentation with boosted performance (Long, Shelhamer, and Darrell 2015; Ren et al. 2015; Chen et al. 2017a,b, 2018; Liu et al. 2019; Wang et al. 2020). However, DNNs usually suffer from severe overfitting problems.

Various classical data augmentation strategies, including random rotation, random scaling and random cropping are proposed (Simonyan and Zisserman 2014; Russakovsky et al. 2015) to reduce overfitting thus with improved performance in most vision tasks. Recently, several works (DeVries and Taylor 2017; Zhang et al. 2017; Yun et al. 2019;

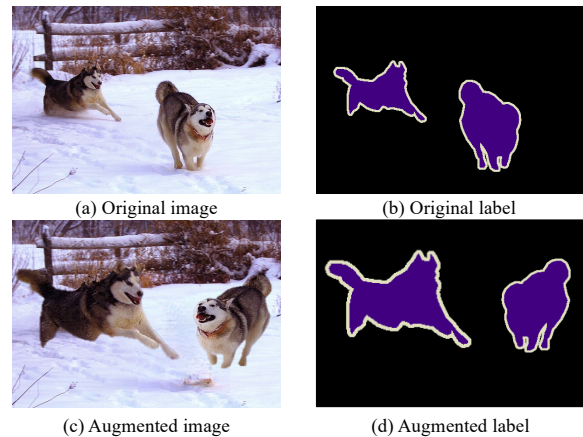


Figure 1: Illustration of ObjectAug. ObjectAug operates at the object level, and can performs various augmentation for each object as shown in (c) and (d). The left husky is scaled and shifted, while the right one is flipped and shifted. Thus, the boundaries are extensively augmented to boost the performance of semantic segmentation.

Zhong et al. 2020; Hendrycks et al. 2019; Guo, Mao, and Zhang 2019a) have pointed out a new direction: mixed data at the image level (a.k.a mixed images) can guide the model to attend on less discriminative parts thus to reduce overfitting. For example, CutOut (DeVries and Taylor 2017) randomly masks out square regions of input during training. While CutMix (Yun et al. 2019) generates a new training sample by randomly combining two cropped training samples. However, both methods operate at the image level, and objects and the background are coupled in the image, which means the boundaries are fixed. Note that boundaries are rather important to obtain precise segmentation (Ding et al. 2019; Kervadec et al. 2019). In this way, the critical boundaries are not augmented well. How can we effectively augment the boundaries in semantic segmentation to further boost the performance?

In this paper, we propose an object-level augmentation method, ObjectAug, to address the above question. As shown in Figure 1, instead of regarding the image as a whole, ObjectAug utilizes the segmentation annotation to decou-

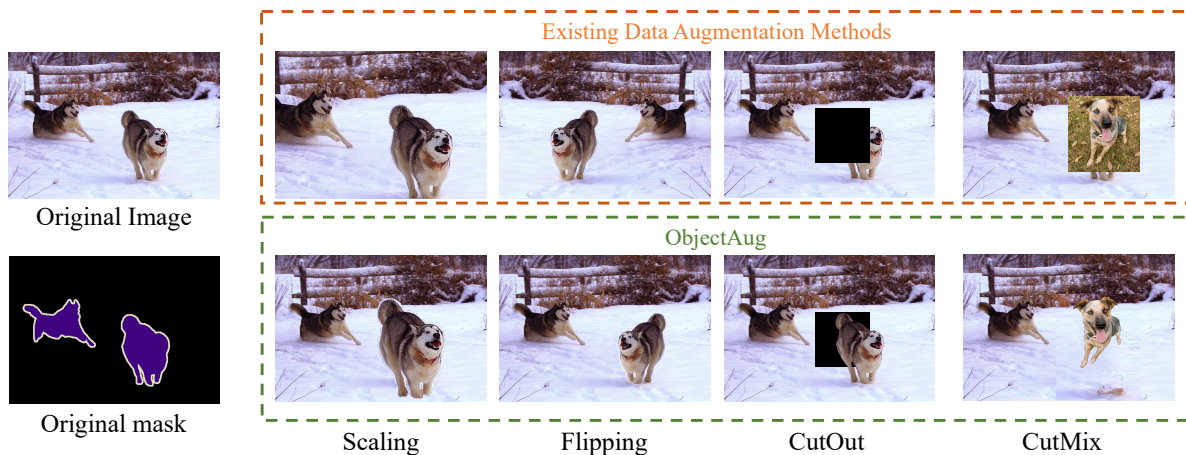


Figure 2: Comparison of ObjectAug and existing data augmentation methods. All the existing methods operate at the image level, while ObjectAug at the object level. ObjectAug can adopt existing methods to augment each object in the image.

ple the image to the background and objects. The object-removed background can be further restored using image inpainting, while the objects can be further augmented independently. Finally, the augmented objects and background are assembled as an augmented image in which objects can be placed flexible on the background. Since the augmentation of objects is performed independently, category-aware augmentation can be easily achieved, e.g., objects in some categories are augmented in every augmented image, while others remain the same (unaugmented) in some augmented images. As existing methods and ObjectAug operate at the image and object levels respectively, the two can be combined to further boost the performance. We present extensive evaluations of ObjectAug on various DNN architectures and datasets on image segmentation. Experiments across various networks and datasets demonstrate that our ObjectAug can improve segmentation performance.

In summary, our contribution can be concluded as follow,

- We propose an object-level data augmentation method, ObjectAug, which can be easily combined with existing methods to further boost performance as existing augmentation methods work at the image level.
- ObjectAug can perform category-aware augmentation to mitigate the category imbalance problems, which performs diversified augmentation methods to objects belongs to different categories.
- Extensive experiment across various networks and datasets demonstrate that ObjectAug outperforms existing data augmentation methods and improve performance significantly.

### Related work

Existing augmentation methods can be divided into two general categories: traditional augmentation methods, and DNN-orientated augmentation methods. In the following, we briefly introduce the two.

The first category has been widely used including random crops, horizontal flipping, and color augmentation

(Krizhevsky, Sutskever, and Hinton 2012a), which improve robustness to situations with translated, reflected, and illuminated objects, respectively. Random scaling (Simonyan and Zisserman 2014) as well as random rotations and affine transformations are also widely adopted. Geometric distortions or deformations are commonly used to increase the number of samples for training DNNs to balance datasets. The above methods have proven to be fast, reproducible, and reliable, and its implementation code is relatively easy and available for the most known deep learning frameworks, which makes it even more widespread (Perez and Wang 2017).

The second category is an emerging trend, which takes the learning characteristics of DNNs into consideration. Mixup (Zhang et al. 2017) uses information from two images. Rather than implanting one portion of an image inside another, Mixup produces an element-wise convex combination of two images. (Guo, Mao, and Zhang 2019b) proposes an adaptive mixing policy to improve Mixup to prevent manifold intrusion. CutOut (DeVries and Taylor 2017) randomly masks out square regions of the input during training, which improves the robustness and overall performance. Rather than occluding a portion of an image, CutMix (Yun et al. 2019) generates a new training sample by randomly combining two cropped training samples. Different from the above methods, AutoAugment (Cubuk et al. 2018) adopted a learning method to get augmentation operations, where a group of augmentation operations is tuned to optimize performance on a downstream task.

In this paper, we compared ObjectAug with both strategies. CutOut and CutMix are selected as representatives of the second category. Note that CutOut and CutMix are primarily for classification and detection tasks, which can be easily revised for segmentation tasks (detailed in the experiment section). Illustration of comparison between ObjectAug, traditional data augmentation methods (scaling and flipping), CutOut and CutMix are shown in Figure 2.

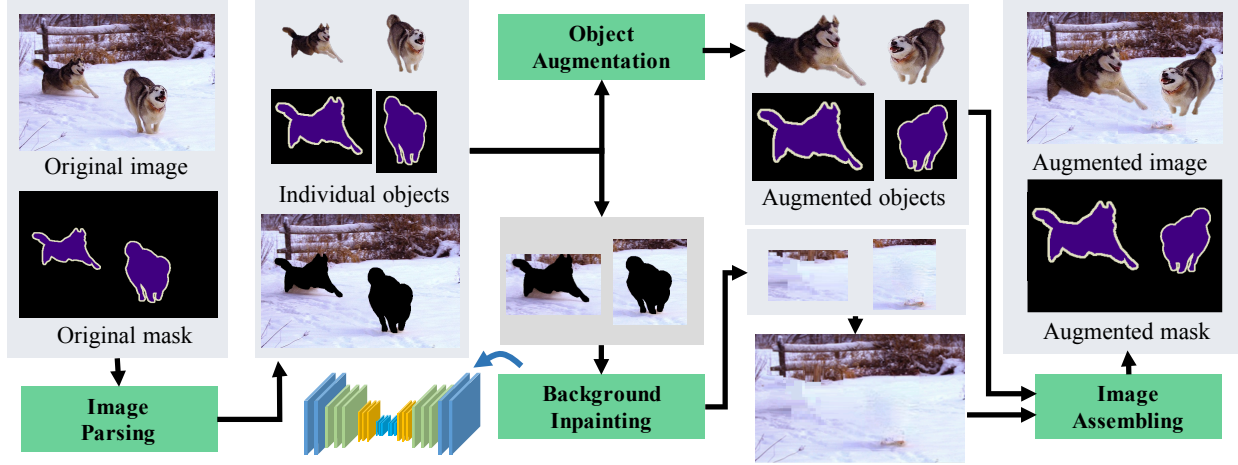


Figure 3: Overall Flow of ObjectAug. ObjectAug includes four modules: image parsing, object augmentation, background inpainting, and image assembling. First, image parsing decouples the image and extracts multiple objects in the image. Next, object augmentation adopts various data augmentation methods to augments the objects. At the same time, background inpainting restores the object-removed background to deal with the black areas. Finally, the augmented objects with restored background and their masks are assembled to obtain the augmented image and mask.

## Method

### Overview

The overall flow of ObjectAug is shown in Figure 3. ObjectAug includes four modules: image parsing, object augmentation, background inpainting, and image assembling. First, image parsing decouples the image and extracts multiple objects in the image. Next, object augmentation performs various data augmentation methods to augments the objects. At the same time, background inpainting restores the object-removed background to deal with the black areas. Finally, the augmented objects, their masks, and restored background are assembled by the image assembling module as the augmented image and mask. We detail the four modules of ObjectAug as follows.

### Image Parsing

Image parsing decouples the image and extracts the objects from the image. For ease of discussion, a training image and its mask are denoted as  $\mathbf{I}$  and  $\mathbf{M}$ , respectively. By utilizing the segmentation annotation, we can easily decouple the mask  $\mathbf{M}$  to  $\mathbf{M}^k \in \{0, 1\}^{W \times H}$ , which is the mask of the  $k$ th object. It associates binary values in the mask to pixels in the image so that  $\mathbf{M}_{x,y}^k = 1$  if the pixel at  $(x, y)$  belongs to the  $k$ th object. Note that since one pixel can only belong to one object, the masks are constrained by Eq. 1.

$$\sum_{k=1}^n \mathbf{M}^k = \mathbf{1}, \quad \mathbf{M}^n = \mathbf{1} - \sum_{k=1}^{n-1} \mathbf{M}^k. \quad (1)$$

The background masks  $\mathbf{M}_n$  can be easily retrieved from the object masks. The process of extracting the  $k$ th object is denoted as  $\mathbf{I}^k \in \mathbb{R}^{W \times H \times C}$ . The decouple of the objects in

an image is computed as follows:

$$\mathbf{I}^k = \mathbf{M}^k \odot \mathbf{I}, \quad \sum_{k=1}^n \mathbf{I}^k = \mathbf{I}. \quad (2)$$

Meanwhile, if traditional data augmentation methods such as rotation or flipping are used directly to the object with its size unchanged, its position may change considerably, which may result in a big black area in the image. In order to minimize the black area brought by ObjectAug, we crop each object  $\mathbf{I}^k$  and its corresponding ground truth  $\mathbf{M}^k$ , and get the cropped object patch  $\mathbf{I}_c^k$  and ground truth  $\mathbf{M}_c^k$ .  $\psi$  denotes the crop parameter, which takes the center of the object as the cropping center, and the crop size is based on the size of the object.

$$\mathbf{I}_c^k, \mathbf{M}_c^k = f_c(\mathbf{I}^k, \mathbf{M}^k | \psi). \quad (3)$$

### Object Augmentation

The object augmentation module augments the extracted objects from the image parsing module individually. Given a series of traditional data augmentation methods including scaling, rotation, shifting, flipping, brightening and etc., denoted as  $[f_1, f_2, \dots, f_m]$ , they are performed to each object with a set of probabilities  $\mathbf{P}=[p_1, p_2, \dots, p_m]$ . Combining them, we get the composed augmentation function  $f_{ObjAug}$ . Applying the composed augmentation method  $f_{ObjAug}$  to the extracted object and mask patches, the augmented objects are finally obtained.

$$f_{ObjAug}(\mathbf{I}|\mathbf{P}) = f_1(\mathbf{I}|p_1) \circ f_2(\mathbf{I}|p_2) \circ \dots \circ f_m(\mathbf{I}|p_m). \quad (4)$$

$$\mathbf{I}_{aug}^k, \mathbf{M}_{aug}^k = f_{ObjAug}(\mathbf{I}_c^k, \mathbf{M}_c^k | \mathbf{P}). \quad (5)$$

As each object can be augmented individually, the object augmentation module can support category-aware augmentation. Note that category imbalance is a common problem in semantic segmentation, and categories that are less and hard to segment are more critical in training. Meanwhile, the data augmentation not only brings generalization to the train samples, it also make it difficult to train. Therefore, an intuitive idea is that the method can be inclined to more rare cases called rarity-driven coefficient so that the model can alleviate under-fitting because of too few examples. However, we actually find that the rarity of objects is not directly proportional to the final segmentation performance. For example, the number of object in category people is far more than that of all other category objects, but its segmentation performance is ranked 13-th. Then we also use the segmentation performance as the criterion of the category-aware coefficient called hard-driven coefficient. We will details the comparison of two coefficients in ablation analysis.

In the hard-driven coefficient, the performance in previous experiment of  $j$ th category is  $N_j$ , and the median score is  $N$ .  $\alpha_j$  is defined as the category-aware coefficient for the  $j$ th category, which is calculated as

$$\alpha_j = \frac{N}{N_j}, \quad (6)$$

where  $N$  and  $N_j$  represent the total number of objects and the number of objects belonging to the  $j$ -th class, respectively, for rarity-driven coefficients. Finally, the probability of the  $j$ th object using augmentation method  $m$  is defined as

$$p_{j,m} = p_m \times \alpha_j. \quad (7)$$

## Background Inpainting

The image parsing module brings black areas in the object-removed background which can not always be covered completely by the augmented object  $I_{aug}^k$ . In addition to filling random noise, we use image inpainting methods to fill the back areas. To prevent the inpainting methods from being affected by objects, we inpaint the background with the object removed. Particularly, we perform morphological processing to expand extracted object masks thus to remove residual edges. We employ the inpainting methods from (Liu et al. 2018) and denote it as  $\Phi(\cdot)$ , which uses DNNs with partial convolutions to deal with irregular holes. The DNNs model for image inpainting is trained on ImageNet (Deng et al. 2009).

$$\mathbf{I}_i^k = \Phi(\mathbf{I}_c, \mathbf{M}_c^k). \quad (8)$$

$\mathbf{I}_i^k$  is the inpainted result from original cropped image  $\mathbf{I}_c$  with selected object  $\mathbf{M}_c^k$  removed. In the inpainting process, the images are all scaled to a uniform size. Meanwhile, since the object is removed and we only inpaint the background, the annotation does not need to be processed accordingly.

## Image Assembling

Image assembling assembles the augmented objects and the restored background into augmented images and masks.

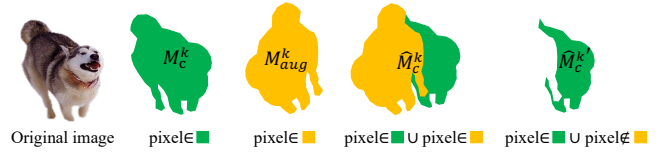


Figure 4: Visualization of masks  $\widehat{\mathbf{M}}_c^k$  and  $\widehat{\mathbf{M}}_c^{k'}$  in the image assembling step.

First, we use the identical cropping parameter  $\psi$  to directly crop the original image  $\mathbf{I}$  and annotation  $\mathbf{M}$  to obtain the cropped image  $\mathbf{I}_c$  and annotation  $\mathbf{M}_c$ .

$$\mathbf{I}_c, \mathbf{M}_c = f_c(\mathbf{I}, \mathbf{M}|\psi). \quad (9)$$

Next, masks of the augmented objects are processed as follows

$$\widehat{\mathbf{M}}_c^k = \mathbf{M}_c^k \cup \mathbf{M}_{aug}^k, \quad \widehat{\mathbf{M}}_c^{k'} = \widehat{\mathbf{M}}_c^k - \mathbf{M}_{aug}^k, \quad (10)$$

where  $\widehat{\mathbf{M}}_c^k$  denotes the union of the original annotation and the augmented annotation for the current image patch  $\mathbf{I}_c$ , and  $\widehat{\mathbf{M}}_c^{k'}$  is the black areas introduced by the misaligned original object and augmented object. For image assembling, the corresponding image area of  $\widehat{\mathbf{M}}_c^k$  is reset (to be black areas), while the corresponding image area of  $\widehat{\mathbf{M}}_c^{k'}$  is restored using image inpainting.

Finally, we assemble the augmented object  $I_{aug}^k$  into the cropped original image as Eq. 11. Meanwhile, the black area is filled with the inpainting results  $\mathbf{I}_i^k$ .

$$\mathbf{I}'_{asm} = \mathbf{I}_c \odot (1 - \widehat{\mathbf{M}}_c^k) + I_{aug}^k + \mathbf{I}_i^k \odot \widehat{\mathbf{M}}_c^{k'}. \quad (11)$$

$$\mathbf{M}_{asm} = \mathbf{M}_c \odot (1 - \widehat{\mathbf{M}}_c^k) + \mathbf{M}_{aug}^k. \quad (12)$$

By assembling the assembled patches  $\mathbf{I}_{asm}$  into the image with the relevant area remove, we get the image with the  $k$ th object augmented. Similarly, we get the corresponding object-level augmented ground truth. Repeat the above process until all objects are processed, and the augmented image and annotation are obtained.

## Experiments

In this section, ObjectAug is extensively evaluated and compared with existing methods on public datasets. First, our experimental setup is described in detail. Second, comparison with CutOut and CutMix, and ablation analysis of hyper-parameter, image inpainting, and category-aware coefficient are performed on the PASCAL VOC 2012 dataset. At last, we further conducted extended experiments on the Cityscapes dataset and CRAG dataset to show the generalizability of our method.

### Experiment Setup

**Datasets** Three image segmentation datasets including PASCAL VOC 2012, Cityscapes, and CRAG are employed for evaluation.

- **PASCAL VOC 2012.** The PASCAL VOC 2012 semantic segmentation benchmark (Everingham et al. 2015) contains 20 foreground object classes. The original dataset contains 1, 464 (train), 1, 449 (val), and 1, 456 (test) pixel-level annotated images. The dataset is augmented by the extra annotations provided by (Hariharan et al. 2011), resulting in 10, 582 (trainaug) training images.
- **Cityscapes.** The Cityscapes dataset (Cordts et al. 2016) is a large-scale dataset containing high-quality pixel-level annotations of 5000 images (2975, 500, and 1525 for training, validation, and test, respectively) and about 20000 coarsely annotated images.
- **CRAG.** The Colorectal Adenocarcinoma Gland (CRAG) dataset (Graham et al. 2019) has a total of 213 H&E CRA images taken from 38 WSIs. Images are at 20× magnification and are mostly of size 1512×1516 pixels, with corresponding instance-level ground truth. The CRAG dataset is split into 173 training images and 40 test images with different cancer grades.

**Implement Details** All experiments were implemented and evaluated on PyTorch platform with Titan X (pascal) with 12 GB memory. For the PASCAL VOC 2012 and cityscapes datasets, we followed the same training protocol as in (Chen et al. 2017b) and refer the interested readers to (Chen et al. 2017b) for details. In short, we employed the same learning rate schedule (i.e., “poly” policy (Liu, Rabinovich, and Berg 2015) and same initial learning rate 0.007), cropped size 513 × 513, fine-tuning batch normalization parameters with output stride 16, and random scale data augmentation during training. Besides, we also used some traditional data augmentation methods including random scale, random shift, random rotation, and random horizontal flip to augment objects in ObjectAug. The specific setting of ObjectAug details in the result and discussion section. The performance was measured in terms of pixel intersection-over-union averaged across all classes (mIOU). For image inpainting, we utilized ResNet50 based U-Net as our model and the loss function from (Liu et al. 2018). We implemented the model with the pre-trained model on ImageNet (Krizhevsky, Sutskever, and Hinton 2012b) and finetuned it on current datasets to enhance the inpainting performance.

## Results on PASCAL VOC 2012

**Effectiveness of ObjectAug** We evaluate ObjectAug based on DeepLabv3 (Chen et al. 2017b) and DeepLabv3plus (Chen et al. 2018) with three backbone model MobileNet (Sandler et al. 2018), ResNet-50 (He et al. 2016), and ResNet-101 on the PASCAL VOC 2012 dataset. Note that all baseline are implemented with traditional data augmentation methods including random scaling, random rotation and random flipping. As shown in Table 1, we can see that ObjectAug improves the mIoU of MobileNet, ResNet-50 and ResNet-101 based DeepLabV3plus by 1.8%, 0.9%, and 1.1%, respectively. Meanwhile, MobileNet, ResNet-50 and ResNet-101 based DeepLabV3 obtain an improvement of 2.4%, 1.6%, and 1.3%, respectively.

Table 1: Performance comparison of models with and without ObjectAug on PASCAL VOC 2012.

Method	Model	ObjectAug	mIoU (%)
DeepLabV3	MobileNet	×	70.1
		✓	<b>71.9</b>
	ResNet-50	×	76.9
		✓	<b>77.8</b>
	ResNet-101	×	77.3
		✓	<b>78.4</b>
DeepLabV3plus	MobileNet	×	71.4
		✓	<b>73.8</b>
	ResNet-50	×	77.2
		✓	<b>78.8</b>
	ResNet-101	×	78.3
		✓	<b>79.6</b>

Table 2: Performance comparison of ObjectAug and traditional data augmentation methods on PASCAL VOC 2012.

Method	Image level	Object level	mIoU (%)
Baseline			68.5
+ R.Rotation	✓		69.8
		✓	69.5
+ R.Scaling	✓		69.9
		✓	70.3
+ R.Flipping	✓		70.1
		✓	69.6
+ R.Shifting	✓		70.3
		✓	70.7
Baseline + All	✓		71.4
Baseline + All		✓	71.2
Baseline + All	✓	✓	73.8

\* All means the combination of the above four data augmentation methods.

**Comparison with Traditional Data Augmentation Methods** In this part, we selected four widely-used traditional data augmentation methods including random rotation, random shifting, random scaling, and random flipping for comparison. Note that the above operations can be performed at two levels: image level (the traditional approach) and object-level in ObjectAug. As shown in Table 2, operation at the object level achieves competition performance with that at the image level. Surprisingly, ObjectAug with random scaling at the object level outperforms that at the image level slightly. On the other hand, we also evaluated the combination of object-level augmentation and image-level augmentation. Notably, we can observe that their combination achieves much better results than each of them, which indicates that ObjectAug has no conflict with traditional data augmentation methods. This may be due to the fact that the two operate at different levels, and thus they can exploit semantic information at different scales with no overlap.

**Comparison with DNN-oriented Methods** We compared our ObjectAug with the current widely-used regular-

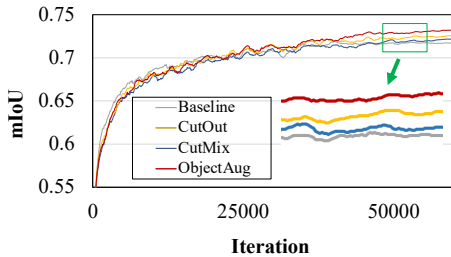


Figure 5: Comparison of mIoU curves over iteration times between CutOut, CutMix, and ObjectAug.

ization technique, CutOut (DeVries and Taylor 2017) and CutMix (Yun et al. 2019). Table 3 details the comparison of our ObjectAug, CutOut, and CutMix. ObjectAug outperforms CutOut 1.5% and CutMix 1.1%, respectively. ObjectAug achieves 73.8% mIoU on PASCAL VOC 2012, 2.5% higher than the baseline of 71.4%. Particularly, the state-of-the-art performance of 74.1% is achieved by combining ObjectAug and CutOut. Figure 5 shows the mIoU curve of them during training, and we can discover that the improvement of ObjectAug is rather stable. Qualitative comparison are shown in Figure 6. Compared with CutOut and CutMix, ObjectAug obtains better performance especially on the boundaries.

Table 3: Performance comparison of ObjectAug and DNN-oriented data augmentation methods on PASCAL VOC 2012. We use MobileNet based DeepLabV3Plus model as our baseline.

Method	mIoU (%)
Baseline	71.4
+ CutOut (16×16, p = 0.5)	71.9
+ CutOut (16×16, p = 1)	72.3
+ CutMix (p = 0.5)	72.7
+ CutMix (p = 1)	72.4
+ ObjectAug	<b>73.8</b>
+ CutOut (16×16, p=0.5) + ObjectAug	73.9
+ CutMix (p=0.5) + ObjectAug	<b>74.1</b>

**Ablation Analysis of Image Inpainting** CutOut and CutMix take different operations on the black areas. In this part, the ablation analysis of the image inpainting module to remove black areas is discussed. As shown in Table 4, we can see that even if there is no processing on the black areas, our ObjectAug can still obtain a significant improvement of 1.7%. In fact, the black area brought by this method can be treated as a unique form of CutOut. Random noise filling also enhances the robustness to some extent. Meanwhile, the inpainting method achieves the best performance among the three processing methods. On the other hand, we also evaluated the training speed of the three methods. We can see that although ObjectAug using the inpainting method can achieve the best performance among the three methods, the speed is 18.5% slower than the baseline.

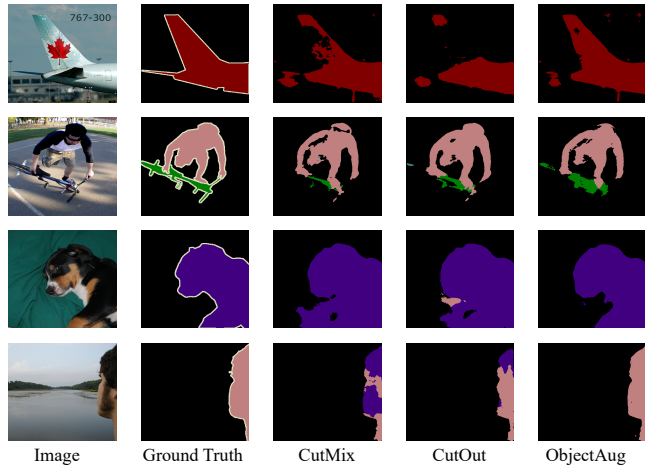


Figure 6: Qualitative comparison of ObjectAug and DNN-oriented data augmentation methods (CutOut, CutMix) on PASCAL VOC 2012.

Table 4: Ablation results of image inpainting.

Method	Speed (s/iter)	mIoU (%)
Baseline	0.698	71.4
+ ObjectAug(w/o fill)	0.721	73.1
+ ObjectAug(random noises)	0.729	73.3
+ ObjectAug(inpainting)	0.827	73.8

**Impact of Category-aware Strategy** Two category-aware strategies: rarity-driven coefficient and hard-driven coefficient are discussed. We introduced two divisions for the 20 categories in PASCAL VOC 2012. In the first division, the first ten (with small number of images) are divided into rare categories group (R), while the last ten (with large number of images) non-rare categories group (NR) to analyze the effect of rarity-driven coefficient. Similarly, the hard categories (H) and the non-hard categories (NH) are obtained to evaluate hard-driven coefficient in the second division. The background is treated as a non-rare and non-hard category. The comparison of two strategies is shown in Table 5. Experimental results show both categories improve the segmentation performance by 1.8-2.4%, and the hard-based rank is more effective (0.8% higher). This is due to the fact that hard cases are more critical to effectively train DNNs.

**Impact of Hyper-parameters** Two groups of hyper-parameters, configurations of each augmentation method and their possibilities, need to be assigned. The first group

Table 5: Result of impact discussion of category-aware coefficient.

Method	H	NH	R	NR	Total
Baseline	57.2	85.6	70.1	72.7	71.4
Rarity-driven	59.3	87.1	70.9	76.7	73.2
Hard-driven	60.2	87.4	70.6	77.0	73.8

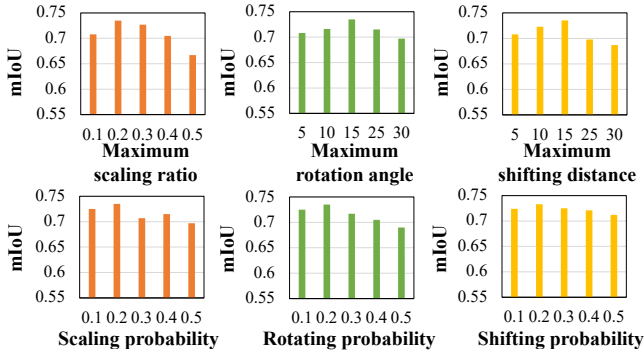


Figure 7: Result of impact discussion of hyper-parameters including random scaling, random rotation and random shift.

Table 6: Performance comparison of models with and without ObjectAug on Cityscapes.

Method	Model	ObjectAug	mIoU (%)
DeepLabV3plus	MobileNet	×	72.0
		✓	73.5
	ResNet-50	×	75.6
		✓	76.9
	ResNet-101	×	77.4
		✓	78.5

includes maximum scaling ratio  $M_z$  in random scaling, maximum rotation angle  $M_s$  in random rotation, and maximum shifting distance  $M_s$  in random shifting. The second is their corresponding probabilities  $P_z, P_r, P_s$ . To demonstrate the impact of these hyper-parameters on the performance, hyper-parameter settings are discussed on DeepLabV3plus (Mobile-Net). We set  $M_z = 1.2, M_r = 15^\circ, M_s = 10$  as the base setting. Results are shown in Figure 7. Notably,  $M_z, M_r,$  and  $M_s$  achieve the optimal performance with  $M_z = 0.2, M_r = 15,$  and  $M_s = 5$ . Meanwhile, their probability of  $[P_z, P_r, P_s]$  demonstrate a better performance with  $[0.2, 0.2, 0.1]$ .

Table 7: Performance comparison of ObjectAug and existing data augmentation methods on Cityscapes.

Method	mIoU (%)
Baseline	72.0
+ CutOut ( $16 \times 16, p = 1$ )	72.8
+ CutMix ( $p = 1$ )	72.6
+ ObjectAug	<b>73.5</b>

### Extended Results on Cityspaces and CRAG

We further evaluated the effectiveness of ObjectAug on hard-to-segment data on the Cityspaces dataset, and its generalization on the CRAG dataset.

**Results on Cityspaces** The hard-to-segment objects belonging to human, vehicle, object, and construction cate-

gories are augmented. As shown in Table 6, we can see that ObjectAug improves MobileNet, ResNet-50 and ResNet-101 based DeepLabV3plus 1.5%, 1.3% and 0.9%. Table 7 shows that ObjectAug also beats CutOut and CutMix by 0.7-0.9%. Compared with CutOut and CutMix with an improvement of 0.8% and 0.6% respectively, the improvement of ObjectAug almost doubles.

Table 8: Performance comparison of models with and without ObjectAug on CRAG.

Method	ObjectAug	mIoU (%)
FCN	×	82.2
	✓	85.5
U-Net	×	84.6
	✓	87.2
PSPNet	×	86.3
	✓	89.1
DeepLabV3	×	87.1
	✓	89.7

**Results on CRAG** Table 8 shows the segmentation performance of FCN, U-Net (Ronneberger, Fischer, and Brox 2015), PSPNet (Zhao et al. 2017), and DeepLabV3 (Chen et al. 2017b) with and without ObjectAug on the CRAG dataset. We can see that ObjectAug can evidently improve the segmentation performance by 2.6-3.3%. As shown in Table 9, compared with other methods, ObjectAug can further improve the performance by 0.7-0.9%. Compared with CutOut and CutMix with an improvement of 0.9% and 0.7% respectively, the improvement of ObjectAug almost doubles.

Table 9: Performance comparison of ObjectAug and existing data augmentation methods on CRAG.

Method	mIoU (%)
Baseline	84.6
+ CutOut ( $16 \times 16, p = 1$ )	85.5
+ CutMix ( $p = 1$ )	85.3
+ ObjectAug	<b>86.2</b>

## Conclusion

In this paper, we proposed a data augmentation method ObjectAug for semantic image segmentation. Unlike existing methods operating at image level, ObjectAug works at object level. In addition, ObjectAug can support category-aware augmentation, and can be easily combined with existing image-level augmentation methods to further enhance performance. Comprehensive experiments are conducted on both natural image and medical image datasets. Experiments cross various models and datasets demonstrate that our ObjectAug outperforms similar works and improve the segmentation performance.

## References

- Chen, L.-C.; Papandreou, G.; Kokkinos, I.; Murphy, K.; and Yuille, A. L. 2017a. Deeplab: Semantic image segmentation with deep convolutional nets, atrous convolution, and fully connected crfs. *IEEE transactions on pattern analysis and machine intelligence* 40(4): 834–848.
- Chen, L.-C.; Papandreou, G.; Schroff, F.; and Adam, H. 2017b. Rethinking atrous convolution for semantic image segmentation. *arXiv preprint arXiv:1706.05587*.
- Chen, L.-C.; Zhu, Y.; Papandreou, G.; Schroff, F.; and Adam, H. 2018. Encoder-decoder with atrous separable convolution for semantic image segmentation. In *Proceedings of the European conference on computer vision (ECCV)*, 801–818.
- Cordts, M.; Omran, M.; Ramos, S.; Rehfeld, T.; Enzweiler, M.; Benenson, R.; Franke, U.; Roth, S.; and Schiele, B. 2016. The cityscapes dataset for semantic urban scene understanding. In *Proceedings of the IEEE conference on computer vision and pattern recognition*, 3213–3223.
- Cubuk, E. D.; Zoph, B.; Mane, D.; Vasudevan, V.; and Le, Q. V. 2018. Autoaugment: Learning augmentation policies from data. *arXiv preprint arXiv:1805.09501*.
- Deng, J.; Dong, W.; Socher, R.; Li, L.-J.; Li, K.; and Fei-Fei, L. 2009. Imagenet: A large-scale hierarchical image database. In *2009 IEEE conference on computer vision and pattern recognition*, 248–255. Ieee.
- DeVries, T.; and Taylor, G. W. 2017. Improved regularization of convolutional neural networks with cutout. *arXiv preprint arXiv:1708.04552*.
- Ding, H.; Jiang, X.; Liu, A. Q.; Thalmann, N. M.; and Wang, G. 2019. Boundary-aware feature propagation for scene segmentation. In *Proceedings of the IEEE International Conference on Computer Vision*, 6819–6829.
- Everingham, M.; Eslami, S. A.; Van Gool, L.; Williams, C. K.; Winn, J.; and Zisserman, A. 2015. The pascal visual object classes challenge: A retrospective. *International journal of computer vision* 111(1): 98–136.
- Graham, S.; Chen, H.; Gamper, J.; Dou, Q.; Heng, P.-A.; Snead, D.; Tsang, Y. W.; and Rajpoot, N. 2019. MILD-net: minimal information loss dilated network for gland instance segmentation in colon histology images. *Medical image analysis* 52: 199–211.
- Guo, H.; Mao, Y.; and Zhang, R. 2019a. Mixup as locally linear out-of-manifold regularization. In *Proceedings of the AAAI Conference on Artificial Intelligence*, volume 33, 3714–3722.
- Guo, H.; Mao, Y.; and Zhang, R. 2019b. Mixup as locally linear out-of-manifold regularization. In *Proceedings of the AAAI Conference on Artificial Intelligence*, volume 33, 3714–3722.
- Hariharan, B.; Arbeláez, P.; Bourdev, L.; Maji, S.; and Malik, J. 2011. Semantic contours from inverse detectors. In *2011 International Conference on Computer Vision*, 991–998. IEEE.
- He, K.; Zhang, X.; Ren, S.; and Sun, J. 2016. Deep residual learning for image recognition. In *Proceedings of the IEEE conference on computer vision and pattern recognition*, 770–778.
- Hendrycks, D.; Mu, N.; Cubuk, E. D.; Zoph, B.; Gilmer, J.; and Lakshminarayanan, B. 2019. Augmix: A simple data processing method to improve robustness and uncertainty. *arXiv preprint arXiv:1912.02781*.
- Kervadec, H.; Bouchtiba, J.; Desrosiers, C.; Granger, E.; Dolz, J.; and Ayed, I. B. 2019. Boundary loss for highly unbalanced segmentation. In *International conference on medical imaging with deep learning*, 285–296.
- Krizhevsky, A.; Sutskever, I.; and Hinton, G. E. 2012a. Imagenet classification with deep convolutional neural networks. In *Advances in neural information processing systems*, 1097–1105.
- Krizhevsky, A.; Sutskever, I.; and Hinton, G. E. 2012b. Imagenet classification with deep convolutional neural networks. In *Advances in neural information processing systems*, 1097–1105.
- Liu, C.; Chen, L.-C.; Schroff, F.; Adam, H.; Hua, W.; Yuille, A. L.; and Fei-Fei, L. 2019. Auto-deeplab: Hierarchical neural architecture search for semantic image segmentation. In *Proceedings of the IEEE conference on computer vision and pattern recognition*, 82–92.
- Liu, G.; Reda, F. A.; Shih, K. J.; Wang, T.-C.; Tao, A.; and Catanzaro, B. 2018. Image inpainting for irregular holes using partial convolutions. In *Proceedings of the European Conference on Computer Vision (ECCV)*, 85–100.
- Liu, W.; Rabinovich, A.; and Berg, A. C. 2015. Parsenet: Looking wider to see better. *arXiv preprint arXiv:1506.04579*.
- Long, J.; Shelhamer, E.; and Darrell, T. 2015. Fully convolutional networks for semantic segmentation. In *Proceedings of the IEEE conference on computer vision and pattern recognition*, 3431–3440.
- Perez, L.; and Wang, J. 2017. The effectiveness of data augmentation in image classification using deep learning. *arXiv preprint arXiv:1712.04621*.
- Ren, S.; He, K.; Girshick, R.; and Sun, J. 2015. Faster r-cnn: Towards real-time object detection with region proposal networks. In *Advances in neural information processing systems*, 91–99.
- Ronneberger, O.; Fischer, P.; and Brox, T. 2015. *U-Net: Convolutional Networks for Biomedical Image Segmentation*. Springer International Publishing.
- Russakovsky, O.; Deng, J.; Su, H.; Krause, J.; Satheesh, S.; Ma, S.; Huang, Z.; Karpathy, A.; Khosla, A.; Bernstein, M.; et al. 2015. Imagenet large scale visual recognition challenge. *International journal of computer vision* 115(3): 211–252.
- Sandler, M.; Howard, A.; Zhu, M.; Zhmoginov, A.; and Chen, L.-C. 2018. Mobilenetv2: Inverted residuals and linear bottlenecks. In *Proceedings of the IEEE conference on computer vision and pattern recognition*, 4510–4520.
- Simonyan, K.; and Zisserman, A. 2014. Very deep convolutional networks for large-scale image recognition. *arXiv preprint arXiv:1409.1556*.
- Wang, J.; Sun, K.; Cheng, T.; Jiang, B.; Deng, C.; Zhao, Y.; Liu, D.; Mu, Y.; Tan, M.; Wang, X.; et al. 2020. Deep high-resolution representation learning for visual recognition. *IEEE transactions on pattern analysis and machine intelligence*.
- Yun, S.; Han, D.; Oh, S. J.; Chun, S.; Choe, J.; and Yoo, Y. 2019. Cutmix: Regularization strategy to train strong classifiers with localizable features. In *Proceedings of the IEEE International Conference on Computer Vision*, 6023–6032.
- Zhang, H.; Cisse, M.; Dauphin, Y. N.; and Lopez-Paz, D. 2017. mixup: Beyond empirical risk minimization. *arXiv preprint arXiv:1710.09412*.
- Zhao, H.; Shi, J.; Qi, X.; Wang, X.; and Jia, J. 2017. Pyramid scene parsing network. In *Proceedings of the IEEE conference on computer vision and pattern recognition*, 2881–2890.
- Zhong, Z.; Zheng, L.; Kang, G.; Li, S.; and Yang, Y. 2020. Random Erasing Data Augmentation. In *AAAI*, 13001–13008.